Available online at www.sciencedirect.com
SCIENCE DIRECT®
Journal of Nuclear Materials 343 (2005) 178–183
journal of nuclear materials
www.elsevier.com/locate/jnucmat

Effect of proton beam profile on stress in JSNS target vessel

Hiroyuki Kogawa *, Syuichi Ishikura, Hiroshi Sato, Masahide Harada, Shunichi Takatama, Masatoshi Futakawa, Katsuhiro Haga, Ryutaro Hino, Shinichiro Meigo, Fujio Maekawa, Yujiro Ikeda

Japan Atomic Energy Research Institute, 2-4 Shirakata-Shirane, Tokai-mura, Naka-gun, Ibaraki-ken 319-1195, Japan

Abstract

A cross-flow type (CFT) mercury target with flow guide blades has been developed for JSNS that suppresses the generation of a stagnant flow region near the beam window where the peak power density is generated due to the spallation reaction. In addition, a flat type beam window has been applied to the CFT target that suppresses dynamic stress caused by pressure waves, that have been estimated with an elastic model for mercury.

Recent experimental results obtained by using a proton beam incident to mercury targets suggested that using a cut-off pressure model for mercury would be appropriate for predicting a dynamic stress behavior in a target vessel. Dynamic stress analyses were carried out with the cutoff pressure model in which the negative pressure less than −0.15 MPa could not be sustained. The dynamic stress generated in the flat beam window became much larger than that in a semi-cylindrical type window as a result of using the cut-off pressure model. Regardless, even the stress generated in the semi-cylindrical type beam window exceeded the allowable stress of SS316L under the peak power density of 668 MW/m^3. In order to decrease the dynamic stress in the semi-cylindrical beam window, the incident proton beam was defocused to reduce the peak power density down to 218 MW/m^3. Although the dynamic stress could be suppressed to less than the allowable stress, the high power density generated on the end of the flow guide blades due to defocus of the proton beam caused high thermal stress exceeding the allowable stress. Several shapes of blade ends were studied analytically to decrease the thermal stress, that did not affect the mercury flow distribution. A simple thin-end blade showed low thermal stress below the allowable stress.

1. Introduction

The Japan Atomic Energy Research Institute (JAERI) is developing a Japanese spallation neutron source (JSNS) with a mercury target in corporation with the High Energy Accelerator Organization (KEK) under Japanese Proton Accelerator Research Complex (J-PARC) project. Fig. 1 shows a schematic drawing of cross flow type (CFT) mercury target that is used in JSNS. In the CFT mercury target, mercury flows across the proton beam along flow guide blades so as to avoid a stagnant region near the target beam window where the high power density is generated by the spallation reaction [1]. The size of the beam window region of the mercury target vessel is 80 mm in height and 260 mm in width. The target vessel is made of 316 L stainless steel.

Mechanical requirement of the target vessel is to withstand the design pressure load, steady thermal stress

* Corresponding author. Fax: +81 29 282 5074.
E-mail address: kogawa@cat.tokai.jaeri.go.jp (H. Kogawa).

0022-3115/$ - see front matter © 2005 Elsevier B.V. All rights reserved.
doi:10.1016/j.jnucmat.2004.08.032

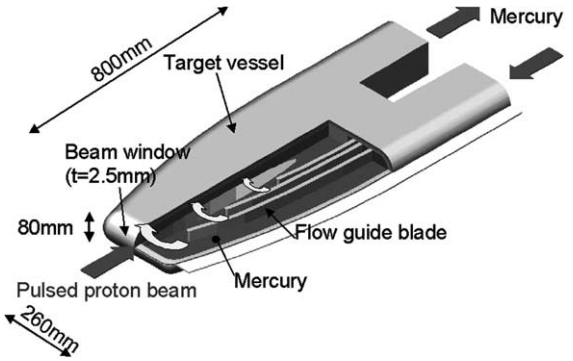

Fig. 1. Schematic drawing of Cross-Flow Type (CFT) mercury target.

and dynamic stress caused by a pressure wave in mercury. The pressure wave was predicted to cause the huge dynamic stress on the beam window. We previously chose a flat type beam window because the generated dynamic stress was lower than that in a semi-cylindrical beam window when an elastic model was assumed as mercury dynamic behavior. In the elastic model, the pressure and the volumetric strain are proportional even when negative pressure was generated [2]. However, it was later announced that the analytical results using a cut-off pressure model represented experimental results well. In the cut-off pressure model, negative pressure less than certain value is not generated even though mercury continues to expand [3].

Ultimately, the generated stress had to be reduced in order to achieve the structural integrity. The analytical results obtained by using the elastic model showed that the stress caused by the pressure waves was decreased with the maximum power density though the total deposition power keeps together [4].

Subsequently the mechanical analyses with the cut-off pressure model were carried out under the various maximum power density conditions to reconsider the shape of the beam window and proton beam profile.

2. Pressure wave and proton beam

Fig. 2(a) shows the analytical model for calculating the dynamic stress. Fig. 2(b) and (c) show schematic drawings of the flat type and the semi-cylindrical type beam windows, respectively. The target vessel wall is mainly 10 mm thick for structural integrity. However, the target beam window is only 2.5 mm thick to suppress thermal stress and absorption of the proton beam. The upper and lower sides of the vessel near the beam window are set at 7.5 mm thick as a compromise between reducing the absorption of generated neutrons by spallation and to keep secure structure. 10 mm thick blades

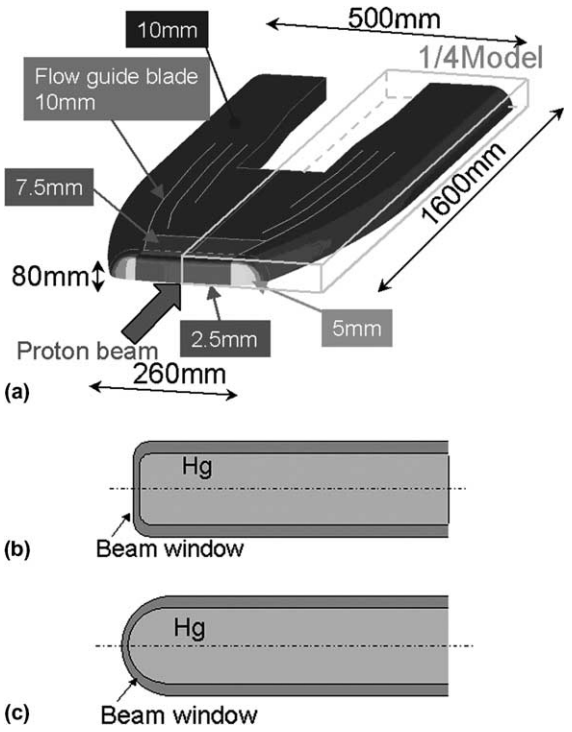

Fig. 2. Analytical model of CFT mercury target: (a) Analytical model of CFT mercury target for dynamic stress, (b) schematic drawing of flat type beam window and (c) schematic drawing of semi-cylindrical type beam window.

function as both the flow guides and as structural members. The dynamic stress analyses were carried out by using the explicit FEM code, LS-DYNA. The analyses were carried out for 1/4 model as shown in Fig. 2(a) considering the symmetry. The vessel was divided into 52 000 shell elements. Mercury inside of the vessel was divided into 663 000 solid elements. Fig. 3 shows mercury models for dynamic stress analyses, that is, the relationship between pressure and volumetric strain of mercury. The thin dashed-line shows the elastic model behavior and the bold line shows the cut-off pressure

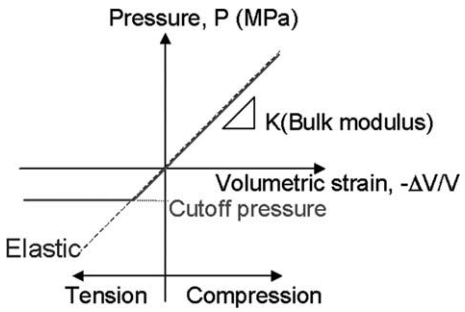

Fig. 3. Mercury model for analyses.

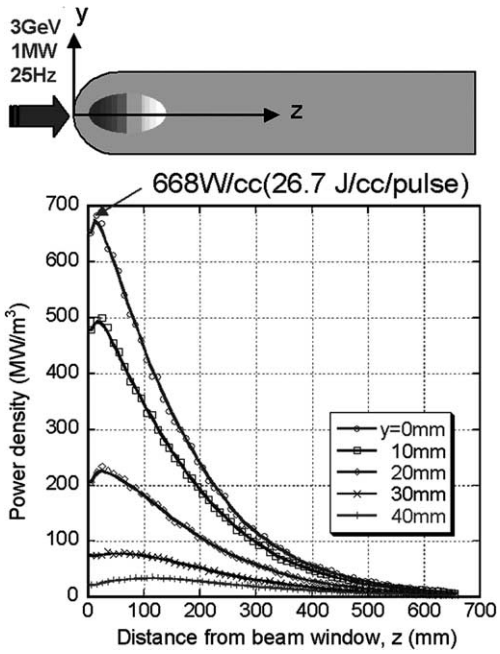

Fig. 4. Power density distribution in mercury on and above proton beam axis.

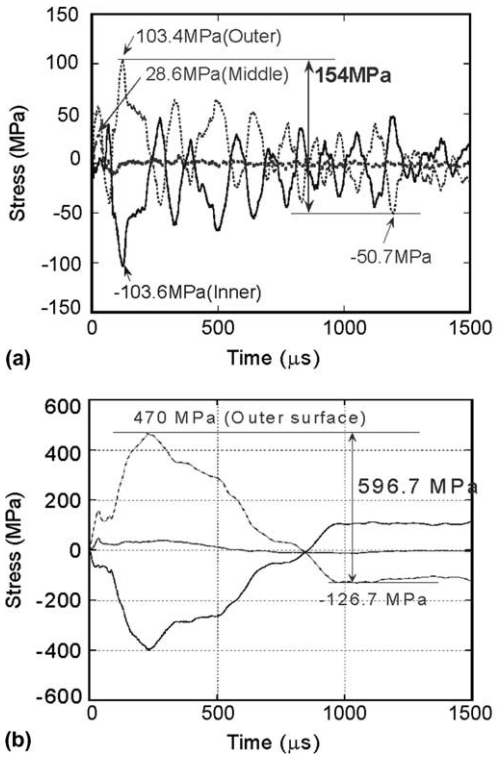

Fig. 5. Stress response at flat type beam window: (a) By using elastic model and (b) by using cut-off pressure model.

model. In these analyses, a cut-off pressure of −0.15 MPa was used based on [3]. Fig. 4 shows a power density distribution in mercury on and above the proton beam axis caused by a Gaussian-profile proton-beam incidence. The maximum power density of 668 MW/m^3 is generated at 30 mm in from the beam window.

Fig. 5 shows the stress response of the vertical component in the flat type beam window comparing effects of mercury model between (a) elastic and (b) cut-off pressure. The generated stress and stress range (the latter effects fatigue life) obtained by the cut-off pressure model shown in Fig. 5(b) is considerably larger than that by the elastic model shown in Fig. 5(a). Stress and stress range obtained by the cut-off pressure model are over the allowable value for the flat type beam window whit Gaussian beam profile. The following reason is considered; the deformation of mercury with the elastic model was constrained due to the stiffness of mercury when mercury tries to expand. Conversely, mercury with the cut-off pressure model does not have stiffness when it expands and continues to load the beam window beyond where the elastic model would. More load into the beam window and vessel results in larger stress and stress range with the cut-off pressure model.

The stress and stress range should be less than the allowable values, even if the assessment of the structural integrity is carried out with the cut-off pressure model. Preliminary analyses with the cut-off pressure model showed the stress caused by the pressure wave decreases with decreasing maximum power density just as the elastic model does. Defocusing the proton beam was then tried to decrease the maximum power density, while maintaining the total deposited power, with aim of decreasing the dynamic stress and stress range. Fig. 6 compares the horizontal distribution of the power density in mercury obtained by the defocused proton beam incidence, otherwise called an expanded uniform profile, with that of the Gaussian profile. The maximum power density was decreased to 218 MW/m^3 from 668 MW/m^3 by changing the beam profile. Fig. 7(a) and (b) show the maximum stress and stress range versus maximum heat density, respectively. Note that JSNS beam pulse frequency is 25 Hz. Fig. 7(a) and (b) also show the effects of both the shape of the beam window and the mercury model. The generated maximum stress and stress range of the flat type beam window was lower than that of the semi-cylindrical type when the elastic model was used for mercury as mentioned in elsewhere [2]. However, the maximum stress and stress range of the flat type was higher than that on the semi-cylindrical type when the cut-off pressure model was used.

Based on the results using the cut-off pressure model, JSNS decided to use the semi-cylindrical type beam window and the expanded uniform beam profile so that the

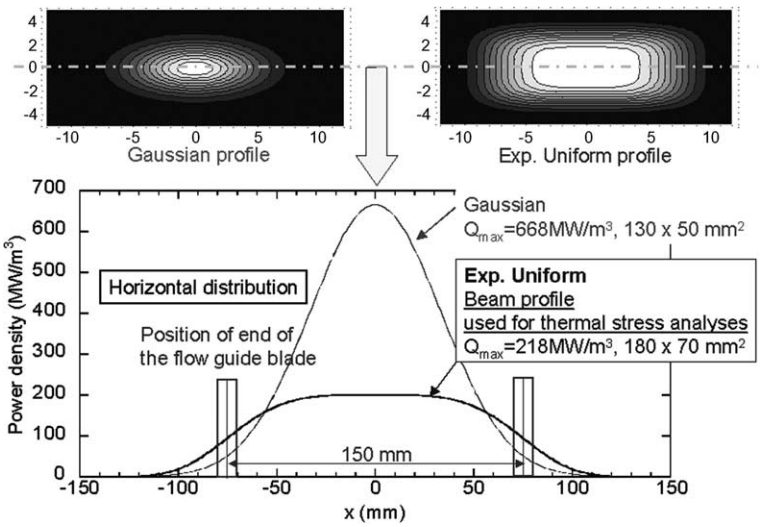

Fig. 6. Power density distribution in mercury in horizontal direction.

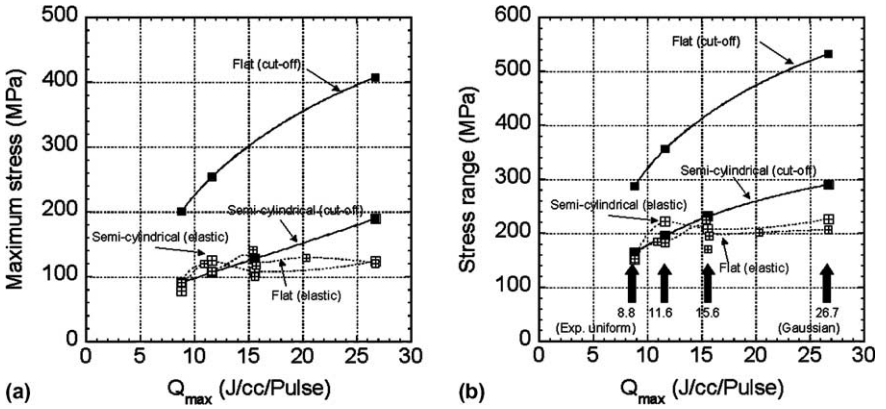

Fig. 7. Maximum stress and stress range with the maximum heat density: Relationship between (a) generated maximum stress and maximum heat density, (b) stress range and maximum heat density.

generated stress and stress range will be less than the allowable limits.

3. Thermal stress and proton beam

The size of the footprint of the expanded uniform proton beam is 180 mm in width and 80 mm in height. On the other hand, the minimum distance between the inlet and outlet flow guide blades in the target vessel is only 150 mm because it was designed for the Gaussian proton beam which size is $130 \times 50\ \mathrm{mm}^2$. The proton beam now directly hits the flow guide blade and the power density at the front end of the blade becomes higher as a result of the defocused proton beam as shown in Fig. 6. This would lead to large thermal stress generation at the front end of the blades. Thermal stress analyses were carried out to assess the structural integrity of the flow guide blades with the expanded uniform beam profile. Fig. 8 shows the half symmetry analytical model for the thermal stress analyses. The half model of the target vessel and the blades were divided into about 64 000 tetra elements with second order. The analyses were carried out by using the commercial FEM code, ABAQUS-Standard. At first, heat transfer analyses were carried out to calculate the temperature distribution in the vessel. The heat transfer coefficient between the target vessel and mercury was set based on the thermal-hydraulic analyses [5]. For example, a heat transfer coefficient of 10 000 $\mathrm{W/m^2/K}$ was set on the beam window, which was not affected by changing the shape of the window to the semi-cylindrical type from the flat type.

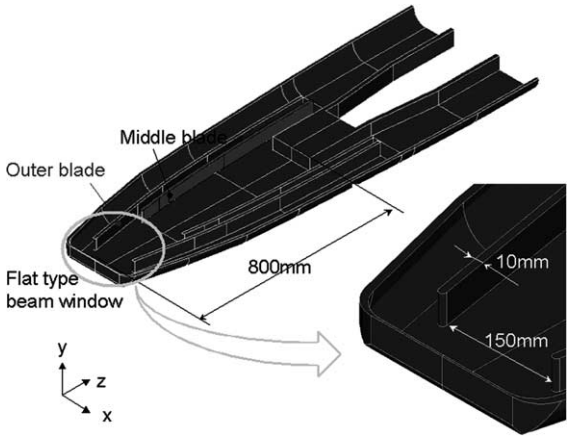

Fig. 8. Analytical model for thermal stress.

Based on the temperature distribution calculated by the heat transfer analyses, thermal stress analyses were carried out.

Fig. 9 shows the thermal stress distribution (Tresca stress) with the flat type beam window caused by the expanded uniform proton beam. The maximum thermal stress at the beam window decreases from 273 MPa [6] to 175 MPa due to the reduced maximum power density. On the other hand, the thermal stress on the front end of the blades increases from almost 0 MPa [6] to 370 MPa which exceeds the allowable stress of the vessel.

The shape of the blades was reconsidered to reduce thermal stress while not effecting the flow distribution of mercury. Fig. 10(a)–(c) show the thermal stress normal component in the horizontal, vertical and proton beam axial direction, respectively, for the same condition shown in Fig. 9. The tensile stress of the vertical component is obviously higher than the other components at the front end of the blades. This is because temperature on the front end of the blades is lower than that inside of the blades as shown in Fig. 11. To reduce the

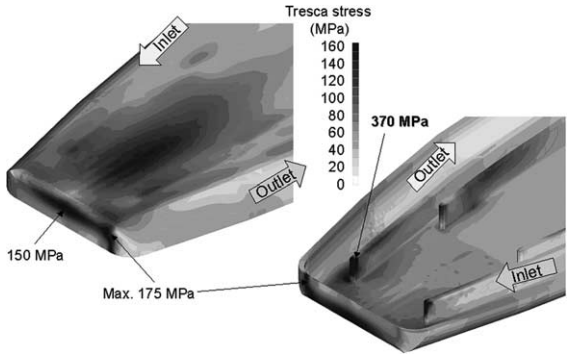

Fig. 9. Thermal stress distribution caused by the expanded uniform profile of proton beam.

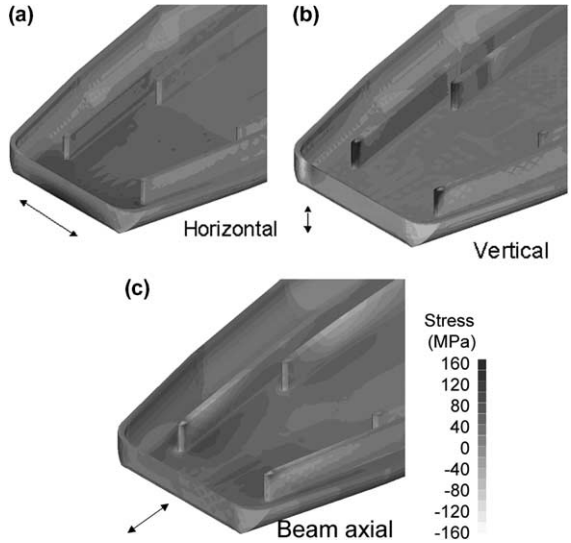

Fig. 10. Distribution of thermal stress normal components: (a) Horizontal direction component, (b) vertical direction component and (c) beam axial direction component.

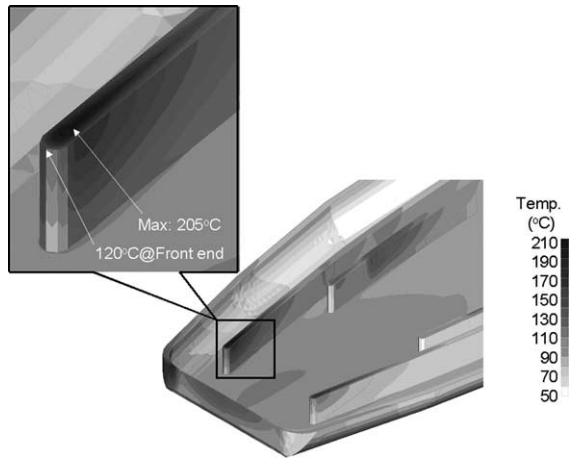

Fig. 11. Temperature distribution caused by the expanded uniform profile of proton beam.

temperature difference between the front end and inside of the blades, the blades were made thinner as shown in Fig. 12. Temperature in the blades is the highest at 10 mm from the front end on the mid-plane as shown in Fig. 11. Ten millimeter blade thickness near the vessel wall is required because the blades will be connected to the vessel by bolts. Away from the vessel wall the thickness is reduced to 6 mm. Fig. 13 shows the thermal stress distribution in the target vessel with the thin front-end blades as shown in Fig. 12 and the semi-cylindrical beam window obtained by the expanded uniform proton beam. The maximum thermal stress on the front end

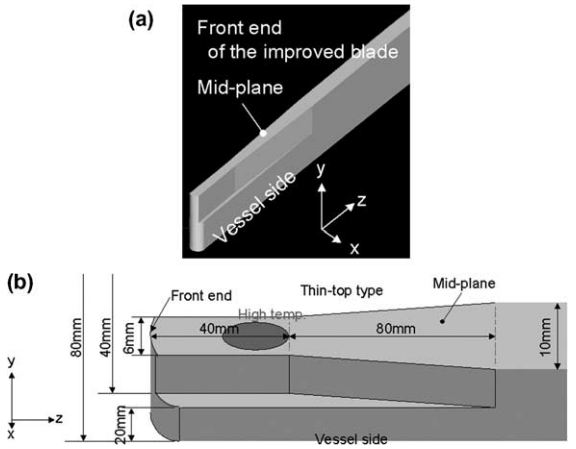

Fig. 12. Improved blade – thin front-end blade – (a) Analytical model and (b) schematic drawing.

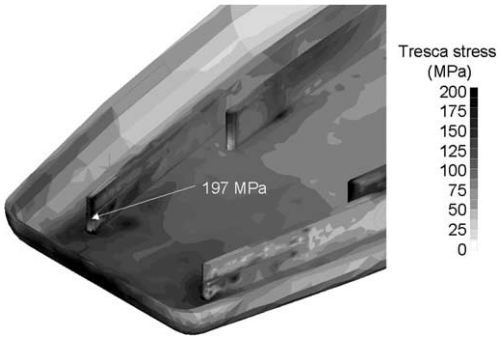

Fig. 13. Thermal stress distribution with thin front-end blade.

of the mercury outlet side blade decreased to 197 MPa from 370 MPa.

4. Structural integrity

To assess the structural integrity under the design condition, the all stress categories, including the primary stress, dynamic stress and the thermal stress must be considered. The structural integrity is assessed by following conditions:

$P < 1.5\mathrm{Sm}$

and

$P + Q + P_{\mathrm{d,max}} < 3\mathrm{Sm},$

where P is the primary stress such as the stress generated by the design pressure, Q the thermal stress, $P_{\mathrm{d,max}}$ the maximum dynamic stress and Sm the allowable stress intensity. In this case, the allowable stress intensity is 115 MPa because the design temperature of the vessel is lower than 150 °C.

The maximum primary stress, P, of 170 MPa was generated at the connection region between the vessel and blade, which is lower than 1.5Sm. The maximum primary and thermal stress in the blade, $(P + Q)_{\max}$, of 197 MPa was generated as shown in Fig. 13. In this study, although the primary and thermal stresses are analyzed simultaneously, the dynamic stress was analyzed by another code. Then the primary and thermal and dynamic stresses, $P + Q + P_{\mathrm{d,max}}$, was calculated by adding the primary and thermal stresses, $(P + Q)_{\max}$, and the dynamic stress, $P_{\mathrm{d,max}}$. The maximum dynamic stress, $P_{\mathrm{d,max}}$, of 80 MPa was generated at the connection region of the vessel and front end of the front blade. Then $(P + Q)_{\max} + P_{\mathrm{d,max}}$ became 277 MPa which was lower than the allowable stress, 3Sm.

5. Concluding remarks

Mechanical analyses were carried out to assess the structural integrity of the mercury target vessel, especially the flow guide blades. The major results of the analyses were:

(1) The dynamic stress and stress range caused by the pressure wave decreased with decreasing maximum heat density. The defocused proton beam is advantageous for dynamic stress as well as thermal stress at the beam window.
(2) The defocused proton beam caused high thermal stress of 370 MPa in the flow guide blade.
(3) Thinning the blade made the temperature difference low between the front-end and inside the blade because the thermal conduction path to mercury became shorter. This thinning also reduced the thermal stress to below the allowable level.

Based on these analyses, JSNS will develop the target design using the semi-cylindrical type beam window and the expanded uniform profile proton beam.

References

[1] K. Haga et al., in: Proceedings of the ICANS-XVI, vol. III, 2003, p. 1315.
[2] H. Kogawa et al., in: Proceedings of the ICANS-XVI, vol. III, 2003, p. 1295.
[3] B.W. Riemer, Benchmark simulations of target vessel strain response to beam induced pressure pulses SNS-101050000-TR0002-R00, 2003.
[4] S. Ishikura et al., Structural integrity of heavy liquid–metal target installed spallation neutron facility – Part 2 : Dynamic stress analysis of target container–, JAERI-Tech 2000-008, 2000, (in Japanese).
[5] H. Satoh, Private communication.
[6] S. Ishikura, Private communication.